Model for phase separation controlled by doping and the internal chemical pressure in different cuprate superconductors

K. I. Kugel and A. L. Rakhmanov
Institute for Theoretical and Applied Electrodynamics, Russian Academy of Sciences, Izhorskaya Str. 13, Moscow, 125412 Russia and Department of Physics, Loughborough University, Loughborough LE11 3TU, United Kingdom

A. O. Sboychakov
Institute for Theoretical and Applied Electrodynamics, Russian Academy of Sciences, Izhorskaya Str. 13, Moscow, 125412 Russia

Nicola Poccia and Antonio Bianconi
Department of Physics, University of Rome "La Sapienza," P. le A. Moro 2, 00185 Rome, Italy
(Received 28 May 2008; revised manuscript received 18 August 2008; published 28 October 2008)

In the framework of a two-band model, we study the phase-separation regime of different kinds of strongly correlated charge carriers as a function of the energy splitting between the two sets of bands. The narrow (wide) band simulates the more localized (more delocalized) type of charge carriers. By assuming that the internal chemical pressure on the CuO_2 layer due to interlayer mismatch controls the energy splitting between the two sets of states, the theoretical predictions are able to reproduce the regime of phase separation at doping higher than 1/8 in the experimental pressure-doping-T_c phase diagram of cuprates at large microstrain as it appears in overoxygenated La_2CuO_4.

DOI: 10.1103/PhysRevB.78.165124 PACS number(s): 71.27.+a, 74.72.−h, 64.75.−g

I. INTRODUCTION

The mechanism driving the emergence of a quantum macroscopic coherent phase that is able to resist to the decoherence effects of high temperature remains a major topic of research in condensed matter. The realization of this macroscopic quantum phase in doped cuprates close to the Mott insulator regime has stimulated a large amount of investigations on the physics of strongly correlated metals. Most theoretical papers treated models of a homogeneous system made of a single electronic band (or models of multiple hybridized bands reduced to a single effective band) with a large Hubbard repulsion.

There is growing agreement that the solution of the problem of high-T_c superconductivity requires the correct description of the normal state where spin, charge, orbital, and lattice degrees of freedom compete and the functional phase emerges in a complex system with two main components showing mesoscopic phase separation. Here we consider a theoretical model of the mesoscopic phase separation in a two-band scenario of two strongly correlated electronic fluids. This simple model grabs the key physics of the anomalous normal phase in cuprates exhibiting the phase separation as a function of charge density and the energy splitting between the two bands. This allows the understanding of the different superconducting phases in different cuprate families, i.e., the three-dimensional (3D) phase diagram where the critical temperature depends on the doping and pressure.[1] The motivation of this theoretical work is based on the results of recent experiments using angular resolved photoemission spectroscopy (ARPES) (Refs. 2–6) and scanning tunneling spectroscopy (STM) (Refs. 7 and 8), providing compelling experimental evidence for the dual nature of charge carriers and the nanoscale phase separation of the two components in two different spatial domains in cuprate high-T_c superconductors.[9–11]

A clear case for the phase separation of the two types of charge carriers is overoxygenated La_2CuO_{4+y}, where the interstitial oxygen ions are mobile above 180 K and stimulate the phase separation of the two different kinds of dopant holes.[12–20] Currently, from the analysis of magnetic neutron scattering experiments, there is an agreement for the frustrated mesoscopic phase separation at doping larger than 1/8 in Sr-doped La214, Y123, and Bi2212 between a first more delocalized component that does not show spin fluctuations and a second more localized electronic component, showing stripelike spin fluctuations.[21,22] Several reviews and books have been published on the two-component scenario and phase separation in cuprates.[18–20,23–26] Here we focus not on the well-studied phase separation in the underdoped regime, near the Mott phase, between a hole-poor antiferromagnetic (AF) phase and a metallic hole-rich phase, but on the phase separation in the overdoped regime[12–22] between a hole-poor phase with doping close to 1/8 and a hole-rich phase with doping close to 1/4.

This phase-separation scenario has been described in Refs. 18, 21, and 22 for LaSrCuO and overoxygenated La_2CuO_4. It is based on the experimental fact that variation in the magnetic incommensurability due to spin stripes saturates at doping 1/8 (see Fig. 15 of Ref. 21). The residual magnetic scattering at high doping suggests that one of the phases has stripe correlations similar to the $x=1/8$ phase with the volume fraction of this phase decreasing with x, as indicated in Fig. 17 of Ref. 21. The other phase is presumably uniformly doped. The picture, then, is that as one increases the doping beyond $x=1/8$, it becomes unfavorable to accommodate the additional holes in stripes; instead, patches of the uniformly doped phase grow at the expense of the stripe phase. The maximum T_c seems to occur in a mixed phase region dominated by the stripe phase.

A similar scenario is now well accepted for understanding the physics of phase separation in manganites.[27–29] It was

shown that even in the absence of any specific order parameter, the presence of two strongly correlated electron bands leads to the possibility of a phase-separated state.[30]

In Ref. 30, the evolution of phase separation was studied as a function of doping. However, a large amount of data clearly indicates that the phase-separation regime is not only a function of doping but also of the anisotropic chemical pressure acting on the CuO_2 layers due to interlayer mismatch.[31–34] The chemical pressure is a well-established physical variable that controls the physical properties of perovskites, and it is usually measured by the average ionic radius of the cations in the intercalated layers or the tolerance factor t; in fact, the internal chemical pressure in perovskites can be defined as $\eta=1-t$. In all perovkites and particularly in manganites, it is well established that the phase diagram of the electronic phases depends on the two variables, charge density and chemical pressure.[35] Since the early years of high-T_c superconductivity research the mismatch chemical pressure has been considered as a key variable controlling the electronic properties of cuprates only on one family, La214;[34] however, it was not possible to extend this idea to other families for the presence of a plurality of intercalated layers with cations having largely different coordination numbers. Therefore, it was not possible to compare the average ionic size $\langle r_A\rangle$ in the intercalated layers and to get the tolerance factor t for all cuprate families. This problem was solved by obtaining the internal chemical pressure from the measure of the compressive microstrain $\varepsilon=(R_0-r)/r$ in the CuO_2 plane (that has the same absolute value as the tensile microstrain in the intercalated layers), where r is the average Cu-O distance and $R_0=0.197$ nm is the unrelaxed Cu-O distance.[31–33] Therefore, the chemical pressure is proportional to the microstrain, $\eta=2\varepsilon$.

In the 3D phase diagram, the phase separation for the overdoped regime in overoxygenated La214 occurs in a family with high chemical pressure close to $\eta=8\%$, while it becomes a frustrated phase separation in the LaSrCuO, Bi2212, and Y123 that are in the range of chemical pressure $7\%>\eta>4\%$; while for cuprates with lower microstrain only very fast critical fluctuations could be present.[31–33] In this paper, we propose a model of a two-component system made of two different strongly correlated electron bands, where the chemical pressure controls the energy splitting between the two bands. The phase separation in the overdoped regime can exist for specific values of the ratio between the bandwidth of the two bands. The critical point for the transition from a frustrated phase separation to a nonfrustrated phase separation can be obtained by tuning the long-range $1/r$ Coulomb repulsion that frustrates the phase separation as going from Sr-doped to oxygen-doped La124.

II. MODEL

The existence of the two types of strongly correlated charge carriers in cuprates can be described in terms of the two-band Hubbard model. The Hamiltonian of such a system can be written as[30]

$$H=-\sum_{\langle\mathbf{nm}\rangle\alpha,\sigma} t_\alpha a^\dagger_{\mathbf{n}\alpha\sigma}a_{\mathbf{m}\alpha\sigma}-\Delta E\sum_{\mathbf{n}\sigma} n_{\mathbf{n}b\sigma}-\mu\sum_{\mathbf{n}\alpha,\sigma} n_{\mathbf{n}\alpha\sigma}+\frac{1}{2}\sum_{\mathbf{n}\alpha,\sigma} U^\alpha n_{\mathbf{n}\alpha\sigma}n_{\mathbf{n}\alpha\bar{\sigma}}+\frac{U'}{2}\sum_{\mathbf{n}\alpha,\sigma\sigma'} n_{\mathbf{n}\alpha\sigma}n_{\mathbf{n}\bar{\alpha}\sigma'}. \quad (1)$$

Here, $a^\dagger_{\mathbf{n}\alpha\sigma}$ and $a_{\mathbf{n}\alpha\sigma}$ are the creation and annihilation operators for electrons corresponding to bands $\alpha=\{a,b\}$ at site $\mathbf{n}$ with spin projection σ, and $n_{\mathbf{n}\alpha\sigma}=a^\dagger_{\mathbf{n}\alpha\sigma}a_{\mathbf{n}\alpha\sigma}$. The symbol $\langle\ldots\rangle$ denotes the summation over the nearest-neighbor sites. The first term in the right-hand side of Eq. (1) corresponds to the kinetic energy of the conduction electrons in bands a and b with the hopping integrals $t_a>t_b$. In our model, we ignore the interband hopping. The second term describes the shift ΔE of the center of band b with respect to the center of band a ($\Delta E>0$ if the center of band b is below the center of band a). The last two terms describe the on-site Coulomb repulsion of two electrons either in the same state (with the Coulomb energy U^α) or in the different states (U'). The bar above α or σ denotes *not* α or *not* σ, respectively. The assumption of the strong electron correlations means that the Coulomb interaction is large, that is, $U^\alpha, U' \gg t_\alpha, \Delta E$. The total number n of electrons per site is a sum of electrons in the a and b states, $n=n_a+n_b$, and μ is the chemical potential. Below, we consider the case $n\leq 1$ relevant to cuprates.

Model (1) predicts a tendency to the phase separation in a certain range of parameters, in particular, in the case when the hopping integrals for a and b bands differ significantly ($t_a>t_b$).[30] This tendency results from the effect of strong correlations giving rise to dependence of the width of one band on the filling of another band. In the absence of the electron correlations ($n\ll 1$), the half width $w_a=zt_a$ of the a band is larger than $w_b=zt_b$ (z is the number of the nearest neighbors of the copper ion). Due to the electron correlations, the relative width of a and b bands can vary significantly.[30]

In the limit of strong correlations, $U^\alpha, U'\to\infty$, we can describe the evolution of the band structure with the change in n and ΔE following the method presented in Ref. 30. We introduce the one-particle Green's function,

$$G_{\alpha\sigma}(\mathbf{n}-\mathbf{n}_0,t-t_0)=-i\langle\hat{T}a_{\mathbf{n}\alpha\sigma}(t)a^\dagger_{\mathbf{n}_0\alpha\sigma}(t_0)\rangle, \quad (2)$$

where $\hat{T}$ is the time-ordering operator. The equations of motion for the one-particle Green's function with the Hamiltonian (1) include the two-particle Green's functions:

$$\mathcal{G}_{\alpha\sigma,\beta\sigma'}(\mathbf{n}-\mathbf{n}_0,t-t_0)=-i\langle\hat{T}a_{\mathbf{n}\alpha\sigma}(t)n_{\mathbf{n}\beta\sigma'}(t)a^\dagger_{\mathbf{n}_0\alpha\sigma}(t_0)\rangle.$$

In the considered limit of strong on-site Coulomb repulsion, the presence of two electrons at the same site is unfavorable, and the two-particle Green's function is of the order of $1/U$, where $U\sim U_\alpha, U'$. The equation of motion for $\mathcal{G}_{\alpha\sigma,\beta\sigma'}$ includes the three-particle terms coming from the commutator of $a_{\mathbf{n}\alpha\sigma}(t)$ with the U terms of the Hamiltonian (1), which are of the order of $1/U^2$ and so on. In these equations, following the Hubbard I approach,[36] we neglect the terms of the order of $1/U^2$ and make the following replacement:

$$\langle \hat{T} a_{\mathbf{n}+\mathbf{m}\alpha\sigma}(t) n_{\mathbf{n}\beta\sigma'}(t) a^{\dagger}_{\mathbf{n}_0\alpha\sigma}(t_0)\rangle$$

$$\rightarrow \langle n_{\mathbf{n}\beta\sigma'}\rangle \langle \hat{T} a_{\mathbf{n}+\mathbf{m}\alpha\sigma}(t) a^{\dagger}_{\mathbf{n}_0\alpha\sigma}(t_0)\rangle.$$

As a result, we derive a closed system for the one- and two-particle Green's functions.[30,36] This system can be solved in a conventional manner by passing from the time-space $(t,\mathbf{r})$ to the frequency-momentum $(\omega,\mathbf{k})$ representation. In the case of superconducting cuprates the total number of electrons per site does not exceed unity, $n \leq 1$. The upper Hubbard sub-bands are empty, and we can proceed to the limit $U_\alpha, U' \rightarrow \infty$. In this case, the one-particle Green's function $G_{\alpha\sigma}$ is independent of U and can be written in the frequency-momentum representation as[29,30]

$$G_{\alpha\sigma}(\mathbf{k},\omega) = \frac{g_{\alpha\sigma}}{\omega + \mu + \Delta E^{\alpha} - g_{\alpha\sigma} w_\alpha \zeta(\mathbf{k})}, \tag{3}$$

where $\Delta E^{\alpha}=0$ for $\alpha=a$ and $\Delta E^{\alpha}=\Delta E$ for $\alpha=b$,

$$g_{\alpha\sigma} = 1 - \sum_{\sigma'} n_{\bar{\alpha}\sigma'} - n_{\alpha\bar{\sigma}}, \tag{4}$$

where $n_{\alpha\sigma}=\langle n_{\mathbf{n}\alpha\sigma}\rangle$ is the average number of electrons per site in the state (α,σ) and $\zeta(\mathbf{k})$ is the spectral function depending on the lattice symmetry. Since the results do not vary crucially with the change of the lattice symmetry,[30] here we consider the case of the simple cubic lattice when $\zeta(\mathbf{k})=-[\cos(k^1 d)+\cos(k^2 d)+\cos(k^3 d)]/3$, where d is the lattice constant. In the main approximation in $1/U$, the magnetic ordering does not appear and we can assume that $n_{\alpha\uparrow}=n_{\alpha\downarrow}\equiv n_\alpha/2$.

Equations (3) and (4) demonstrate that the filling of band a depends on the filling of band b and vice versa. Indeed, using the expression for the density of states $\rho_\alpha(E)=-\pi^{-1}\,\mathrm{Im}\int G_\alpha(\mathbf{k},E+i0)d^3\mathbf{k}/(2\pi)^3$, we get the following expression for the numbers of electrons in bands a and b $(\alpha=a,b)$:

$$n_\alpha = 2 g_\alpha n_0\left(\frac{\mu + \Delta E^{\alpha}}{g_\alpha w_\alpha}\right), \tag{5}$$

where

$$n_0(\mu') = \int_{-1}^{\mu'} dE' \rho_0(E'), \tag{6}$$

and $\rho_0(E')=\int d^3\mathbf{k}\,\delta[E'-\zeta(\mathbf{k})]/(2\pi)^3$ is the density of states for free electrons (with the energy normalized by unity, $|E| \leq 1$). The chemical potential μ in Eq. (5) can be found from the equality $n=n_a+n_b$.

When the energy band b is far above the center of band a $(\Delta E<0)$, there exist only a electrons. With the increase in ΔE, the chemical potential reaches the bottom of the b band $-\Delta E - w_b$. At higher ΔE, the b electrons appear in the system, and the effective width of the a band, $w_a^{\mathrm{eff}}=2w_a g_a$, starts to decrease. At large positive values of ΔE, the a carriers in the system disappear and there exist only b electrons. The plots of n_a, n_b, and the effective bandwidth as functions of ΔE are shown in Figs. 1 and 2, respectively.

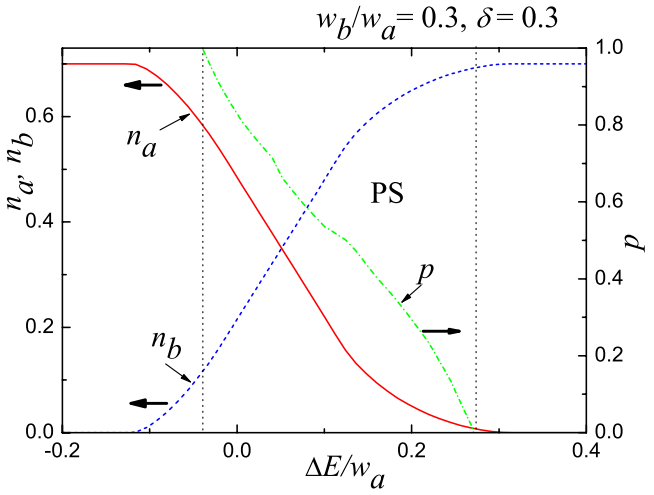

FIG. 1. (Color online) Evolution of the occupation numbers n_a and n_b of the bands a and b at fixed doping $\delta=1-n=0.3$ in the absence of phase separation. The region of phase separation lies between two vertical dotted lines. There we have two phases: P_a including mostly a charge carriers and P_b with dominant b carriers. The content of different types of carriers in P_a and P_b is given by the intersections of n_a and n_b curves with left and right dashed vertical curves, respectively. The change in concentration p of phase P_a in the phase-separation region is shown by the (green) dot-dashed line.

The energy of the system in the homogeneous state, E_{hom}, is the sum of electron energies in all filled bands. Similarly to Eq. (5), we can write E_{hom} in the form

$$E_{\mathrm{hom}} = 2\sum_\alpha g_\alpha^2 w_\alpha \varepsilon_0\left(\frac{\mu + \Delta E^{\alpha}}{g_\alpha w_\alpha}\right) - \Delta E n_b, \tag{7}$$

where

$$\varepsilon_0(\mu') = \int_{-1}^{\mu'} dE' E' \rho_0(E'). \tag{8}$$

The dependence of $E_{\mathrm{hom}}(n)$ is shown in Fig. 3 at different values of ΔE. We see that within a certain n range, the sys-

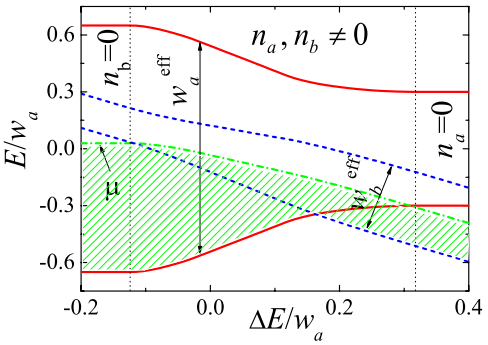

FIG. 2. (Color online) Effective widths $w_{a,b}^{\mathrm{eff}}$ of the a and b bands versus band shift ΔE at fixed doping $\delta=1-n=0.3$. The (green) dot-dashed curve illustrates the behavior of the chemical potential μ; the (green) hatched area under this curve corresponds to the states occupied by charge carriers.

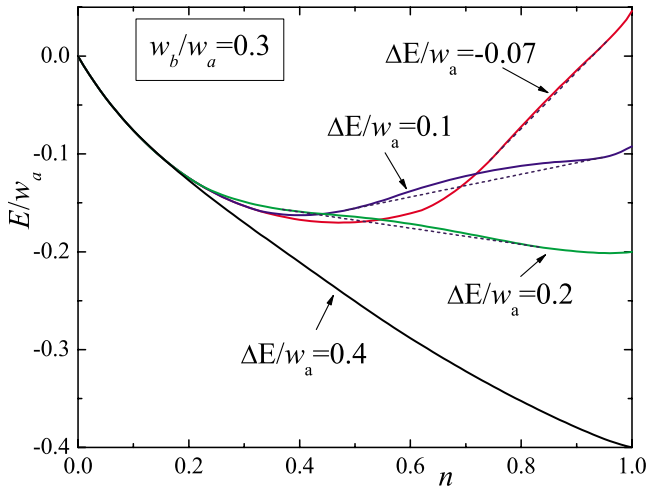

FIG. 3. (Color online) The energy of the system vs doping level n at different values of ΔE. Solid curves correspond to the homogeneous state, whereas the dashed curves are the energies of the phase-separated state without taking into account electrostatic and surface contributions to the total energy.

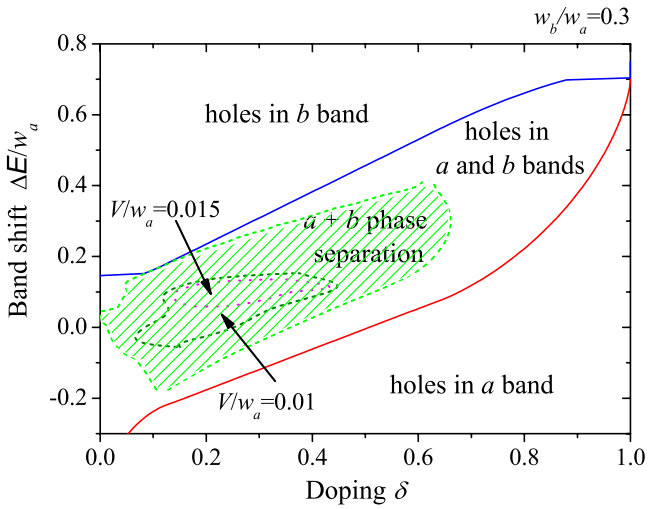

FIG. 4. (Color online) The phase diagram of model (1) in the (doping, band shift) plane at the ratio of bandwidths w_b/w_a=0.3. Below the lower (red) solid line, there are charge carriers only of a type, whereas above the upper (blue) curve, only b carriers. Between these lines, there appears the region of phase separation [marked by (green) hatching]. The charge disproportionalization in the phase-separated state can substantially reduce this region: the arrows indicate the phase-separation regions at V/w_a=0.01 and 0.015, where V is the characteristic energy of intersite Coulomb interaction.

tem can have a negative compressibility, $\partial^2 E_{\text{hom}}/\partial n^2 < 0$, which means a possibility for the charge carriers to form two phases with different electron concentrations.[30,31] The negative compressibility disappears when the centers of the bands are far apart from each other (see, e.g., the curve corresponding to $\Delta E/w_a$=0.4 in Fig. 3).

The phase separation may be hindered by increase in the total energy due to surface effects and a charge redistribution. However, at first we do not take into account these effects. We consider two phases, P_a (low carrier density) and P_b (high carrier density), with the number of electrons per site n_1 and n_2, respectively. A fraction p of the system volume is occupied by the phase P_a and $1-p$ is a fraction of the phase P_b. We seek a minimum of the system energy

$$E^0_{ps}(n_1,n_2) = pE_{\text{hom}}(n_1) + (1-p)E_{\text{hom}}(n_2) \tag{9}$$

under the condition of the charge carrier conservation $n = pn_1 + (1-p)n_2$. The results of calculations of the system energy in the phase-separated state are shown in Fig. 3 by the dashed lines. We see that the phase separation exists in the range of n where both types of charge carriers coexist in the homogeneous state. The ratio of the numbers of a and b carriers is different in different phases. In the first phase P_a, almost all charge carriers are in band a, while in the second phase P_b the situation is opposite.

The redistribution of charge carriers in the phase-separated state gives rise to the additional electrostatic contribution, E_C, to the total energy. This term in the Wigner-Seitz approximation was calculated in Ref. 30. At $p<0.5$ it can be written as $E_C = V(n_1-n_2)^2(R_s/d)^2 u(p)$, where

$$u(p) = 2\pi p(2 - 3p^{1/3} + p)/5, \tag{10}$$

V is the characteristic energy of the intersite Coulomb interaction and R_s is the radius of the spherical droplet of the phase P_a surrounded by the shell of the phase P_b. In the case $p>0.5$, we should replace $n_1 \leftrightarrow n_2$ and $p \leftrightarrow 1-p$. The second contribution to the total energy, depending on the size of inhomogeneities, is related to the surface between the two phases. The corresponding energy per unit volume can be presented in the form $E_S = pS\sigma(n_1,n_2)/V_0$, where $p<0.5$, S is the surface, V_0 is the volume of the inhomogeneity, and $\sigma(n_1,n_2)$ is the surface tension. For spherical droplets, we have $E_S = 3p\sigma(n_1,n_2)d/R_s$. If $p>0.5$, we should replace $p \to 1-p$. Minimization of the sum $E_{CS} = E_C + E_S$ with respect to R_s allows us to calculate this value. In doing so, we get at $p<0.5$

$$R_s = d\left(\frac{3p\sigma(n_1,n_2)}{2V_0(n_2-n_1)^2 u(p)}\right)^{1/3}. \tag{11}$$

The total energy of the inhomogeneous state then reads

$$E_{ps} = pE_{\text{hom}}(n_1) + (1-p)E_{\text{hom}}(n_2) + E_{CS}(R_s), \tag{12}$$

where R_s is given by Eq. (11). The surface energy comes from the size quantization and it was estimated in Ref. 30. The electrostatic and surface contributions to the energy related to an inhomogeneous charge distribution reduce the range of n, in which the phase separation is favorable (see the phase diagram in Fig. 4).

III. RESULTS AND DISCUSSION

The undoped state of the cuprates corresponds to one electron per site (n=1) in the model used in Ref. 30. The number of itinerant holes δ is related to n as $\delta = 1-n$. In general, the relationship between n and δ could be more complicated;[37] however, for the present considerations such

corrections are not of principal importance. The phase diagram of model (1) in the $(\delta,\Delta E)$ plane is drawn in Fig. 4. In this figure, below the lower (red) solid line, we have the charge carriers only of a type, whereas above the upper (blue) curve, there are only b carriers. If we ignore the possibility of the phase separation, the relative number of a and b charge carriers varies gradually between these two lines. The evolution of the occupation numbers n_a and n_b of the two bands with ΔE at a fixed doping is illustrated in Fig. 1. Note also that the effective widths of the a and b bands also vary with the band shift due to the electron correlation effects. This is illustrated in Fig. 2. Taking into account possible phase-separated states results in a significant modification of the phase diagram in the range of intermediate doping. In the hatched (green) region in Fig. 4 the homogeneous state becomes unfavorable, and the system separates into two phases (P_a and P_b) with different numbers of charge carriers per site $n_1 \approx n_a$ and $n_2 \approx n_b$. The electrostatic contribution to the energy related to an inhomogeneous charge distribution reduces the doping range, in which the phase separation is favorable.[30] In Fig. 4, we illustrate that a relatively small energy loss due to the charge disproportionalization leads to a substantial decrease in the area of the phase-separation region: compare the areas indicated by arrows corresponding to $V/w_a=0.01$ and 0.015 (V is the characteristic energy of intersite Coulomb interaction[38]) and the whole hatched area corresponding to $V=0$. Note that at low hole doping (n close to one), the AF correlations are dominant, which requires a special analysis.

Estimating the contribution of the long-range Coulomb interaction to the energy of the phase-separated state, we assume the simplest dropletlike geometry of the inhomogeneities. The phase separation occurs in the range of parameters where the energy of the homogeneous state as a function of doping has a negative curvature corresponding to the negative compressibility.[29,30] It was widely discussed in the literature that long-range Coulomb interaction in the systems with negative compressibility can give rise to more complicated geometry of the phase separation (stripes, layers, rods, etc.) (see Refs. 39 and 40 and references therein). Thus, a due account of the long-range Coulomb interaction could reproduce different superstructures (stripes, in particular) observed in the cuprate superconductors near the optimum doping. However, the proper analysis of the inhomogeneity geometry requires a further study based on a more complicated model.

Now let us discuss the relation of the above model to the experimental situation in the copper-based perovskites, where two types of charge carriers and the inhomogeneous (phase-separated) state are observed. The inhomogeneous state in cuprates corresponds to the coexistence of two phases. One of them is characterized by a superstructure (charge ordering, stripes, etc.) and another one has no superstructure. The state with charge (or spin) superstructure corresponds to a higher degree of localization and, therefore, to a smaller value of the hopping integral. Naturally, a charge carrier may hop either retaining short-range order and gaining in the potential energy or hop in an arbitrary way with larger hopping integral, thus gaining in the kinetic energy. The former corresponds to our b state and the latter to the a state. In our analysis, we did not consider any ordering, which arises in the next-order approximations. In particular, magnetic order requires taking into account the terms of the order of $t_{a,b}^2/U$, and the charge ordering implies allowing for the Coulomb interaction of carriers at different sites (nearest-neighbor at least).

The relative position of the two bands, ΔE, and hopping integrals, $t_{a,b}$, depends, in particular, on the chemical pressure proportional to a microstrain ε in the crystal lattice. To describe the experimental phase diagram of cuprates in the (δ,ε) plane,[1,31–33] we should know the relationship between the model parameters and the chemical pressure. It is natural to assume that the two bands in the cuprate crystal originate from the double degenerate e_g hole level of Cu^{2+} (configuration d^9) in the crystal field of cubic symmetry. The splitting of this level occurs due to lattice distortions related to the Jahn-Teller effect, lowering the cubic symmetry. The chemical pressure distorts the crystal lattice even more and should affect the value of ΔE significantly. It is natural to assume that ΔE and ε are linearly related to each other, if $|\varepsilon| \ll 1$. So, we can write

$$\Delta E(\varepsilon) = \Delta E(0) + \Delta E_1 f(\varepsilon), \tag{13}$$

where $f(\varepsilon)$ is a dimensionless function and $f(\varepsilon) \approx \varepsilon$ at $|\varepsilon| \ll 1$. Cu^{2+} is a typical Jahn-Teller ion, and we can assume that ΔE_1 is of the order of the characteristic Jahn-Teller energy, which is larger than t_a (see, e.g., Refs. 30, 38, and 41 and references therein). The effect of the microstrain on the relative band positions can be significant since the value ΔE arises due to splitting of the originally degenerate levels. At the same time, small strains give rise only to small corrections to the bandwidth. So, the ratio t_b/t_a is considered further on as independent of ε. Note also that the values of the intersite Coulomb interaction V characteristic of perovskites is of the order of $0.1-0.01t_a$ (see, e.g., Ref. 38 and references therein). Thus, the value $V=0.015zt_a$ used below is quite reasonable.

Bearing this in mind, we compare the theoretical phase diagram in Fig. 4 with the experimental 3D phase diagram of cuprates[1,31] in Fig. 5. The left-hand y scale is the mismatch chemical pressure η related to microstrain as $\eta=2\varepsilon$ and the x axis is the doping (the number of holes per Cu site). The color plot represents the values of critical temperature in different superconducting cuprate families. The plot shows the fit of the experimental data of a large number of materials with the convolution of a parabolic curve with the maximum at $T_{\max}$ for T_c as a function of doping, and an asymmetric Lorentzian for $T_{\max}$ as a function of the mismatch chemical pressure with the maximum of 135 K at $2\varepsilon=4\%$. The y axis in the right-hand side of the figure gives the energy distance ΔE between the center of band a and band b normalized to the width of band w_a of the more itinerant carriers. The phase diagram involving the superconducting critical temperature, chemical pressure, and doping reaches the T_c maximum at $2\varepsilon=4\%$ and 0.16 holes per Cu sites. Based on the aforementioned consideration, we can take $\Delta E(0)=-0.133w_a$ and $\Delta E(0)=6.67w_a$ in Eq. (13). We can identify a low-doping insulating phase, for any chemical pressure, at doping smaller than 0.06, where the vertical dashed line indicates

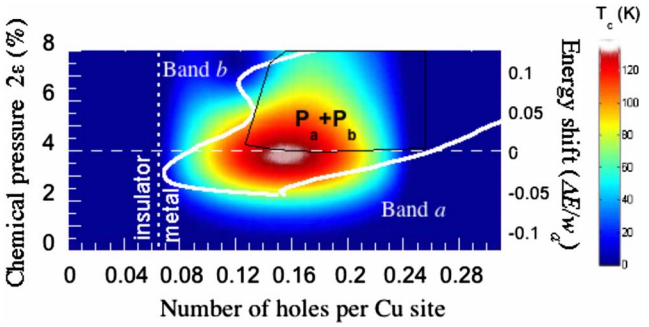

FIG. 5. (Color online) The values of superconducting transition temperature T_c, from 0 at the edge to 135 K in the center, is shown in a color plot as function of chemical pressure (2ε) and doping (number of holes per Cu site). The white curve corresponds to the phase-separation region given by the two-band Hubbard model [Eq. (1)] corresponding to $w_b/w_a=0.3$ and $V/w_a=0.01$ (see Fig. 4). Phases P_a and P_b include mostly the carriers of a and b types, respectively. The black solid line is the boundary of the phase-separated state deduced from neutron scattering and anomalous diffraction experiments for cuprates (La214, Bi2212, and Y123 systems).

the line of the metal-insulator transition. The experimental investigations of the 3D phase diagram of cuprates indicate that the homogeneous metallic phase, with more delocalized states, occurs for both high doping and low chemical pressure, i.e., in the low right corner of the figure. In this region, we have in the theoretical model the charge carriers only in the band a. On the contrary, the homogeneous phase made of localized states, where the striped phase appears, occurs at the corner on the top-left side of the figure. In the theoretical model, we have in such a region the charge carriers only in the band b. The superconducting phase occurs in the intermediate region between these two limiting cases. The phase-separation region predicted by our model (inside the area bounded by the solid white line) corresponds to the superconducting phase. It is in qualitative agreement with the STM, extended x-ray absorption fine structure (EXAFS), and neutron pair distribution function (PDF) experiments, showing that high-T_c superconductivity occurs in a regime of mesoscopic phase separation. The present results show that the maximum critical temperature occurs where the energy splitting between the more itinerant band a and the more localized band b is close to zero.

The theoretical phase diagram reproduces qualitatively the experimental results on the phase separation in cuprates (La214, Bi2212, and Y123 systems) near optimum doping obtained by neutron scattering and anomalous diffraction techniques.[31–33] The phase separation arises in the intermediate doping range and disappears at low and high doping levels. The phase with "more itinerant" electrons exists at small microstrains, the "more localized" (and more ordered) phase arises at higher microstrains, and the phase-separated state is located in the intermediate range of ε. However, our calculations predict the phase separation in a broader doping range than in the experiments. It seems to be a consequence of simplifications used in the formulation and approximate analysis of the two-band Hubbard model [Eq. (1)]. To improve the agreement with the experiment it is necessary to take into account specific features of the lattice and electron structure of the cuprate superconductors. In particular, we disregard the interband electron transitions, that is, we neglect the terms $t_{ab}a^{\dagger}_{\mathbf{n}a\sigma}a_{\mathbf{m}b\sigma}$ in the Hamiltonian (1) assuming that $t_{ab}=0$. The doping range where the phase separation can exist reduces with the increase in t_{ab}.[41]

As it follows from Fig. 5, the superconducting transition temperature T_c is the highest for the parameter range where the system is in the phase-separated state. This is an indication that the mechanism of the phase separation is intimately related to the phenomenon of superconductivity. It is worth to note that in the case when interband coupling t_{ab} is in the range $t_a<t_{ab}<t_b$, the electron density of states has a peak near the Fermi level in the parameter range corresponding to the phase-separated state, where T_c is maximum.[41] We cannot claim whether this fact is accidental or not.

IV. CONCLUSIONS

Up to now, most of the attention both of experimentalists and theorists has been addressed to the phase separation in the underdoped regime between a first undoped antiferromagnetic phase and a second doped metallic phase of cuprates. Now, we have evidence for mesoscopic phase separation in the overdoped region of cuprate superconductors where a striped phase at doping 1/8 coexist with a metallic phase with doping close to 1/4. In our paper, we were dealing just with this situation.

We have presented an emerging theoretical scenario that relates the phase separation to the chemical pressure. This scenario grabs key physical aspects of the 3D phase diagram of cuprates. It was shown that the two-band model is appropriate for the normal phase of all cuprate superconducting families, where the energy splitting between the two bands is controlled by mismatch chemical pressure. In the regime where the two bands are close in energy, the system is unstable toward the phase separation. The highest critical temperature of the superconducting transition in cuprates is attained within the phase-separated state.

ACKNOWLEDGMENTS

The work was supported by the European project CoMePhS (Contract No. NNP4-CT-2005-517039), the International Science and Technology Center (Grant No. G1335), and by the Russian Foundation for Basic Research (Grants No. 08-02-00212 and No. 06-02-16691). A. O. S. also acknowledges support from the Russian Science Support Foundation.

[1] M. Fratini, N. Poccia, and A. Bianconi, J. Phys.: Conf. Ser. **108**, 012036 (2008).
[2] W. S. Lee, I. M. Vishik, K. Tanaka, D. H. Lu, T. Sasagawa, N. Nagaosa, T. P. Deveraux, Z. Hussain, and Z. X. Shen, Nature (London) **450**, 81 (2007).
[3] T. Kondo, T. Takeuchi, A. Kaminski, S. Tsuda, and S. Shin, Phys. Rev. Lett. **98**, 267004 (2007).
[4] M. Le Tacon, A. Sacuto, A. Georges, G. Kotliar, Y. Gallais, D. Colson, and A. Forget, Nat. Phys. **2**, 537 (2006).
[5] K. M. Shen, F. Ronning, D. H. Lu, F. Baumberger, N. J. C. Ingle, W. S. Lee, W. Meevasana, Y. Kohsaka, M. Azuma, M. Takano, H. Takagi, and Z.-X. Shen, Science **307**, 901 (2005).
[6] G. H. Gweon, T. Sasagawa, S. Y. Zhou, J. Graf, H. Takagi, D.-H. Lee, and A. Lanzara, Nature (London) **430**, 187 (2004).
[7] K. McElroy, J. Lee, J. A. Slezak, D.-H. Lee, H. Eisaki, S. Uchida, and J. C. Davis, Science **309**, 1048 (2005).
[8] M. C. Boyer, W. D. Wise, K. Chatterjee, M. Yi, T. Kondo, T. Takeuchi, H. Ikuta, and E. W. Hudson, Nat. Phys. **3**, 802 (2007).
[9] A. Bianconi, N. L. Saini, A. Lanzara, M. Missori, T. Rossetti, H. Oyanagi, H. Yamaguchi, K. Oka, and T. Ito, Phys. Rev. Lett. **76**, 3412 (1996); A. Bianconi, N. L. Saini, T. Rossetti, A. Lanzara, A. Perali, M. Missori, H. Oyanagi, H. Yamaguchi, Y. Nishihara, and D. H. Ha, Phys. Rev. B **54**, 12018 (1996).
[10] K. A. Müller, Guo-meng Zhao, K. Conder, and H. Keller, J. Phys.: Condens. Matter **10**, L291 (1998).
[11] A. Bianconi, Solid State Commun. **91**, 1 (1994).
[12] Y. S. Lee, R. J. Birgeneau, M. A. Kastner, Y. Endoh, S. Wakimoto, K. Yamada, R. W. Erwin, S.-H. Lee, and G. Shirane, Phys. Rev. B **60**, 3643 (1999).
[13] D. Di Castro, M. Colapietro, and G. Bianconi, Int. J. Mod. Phys. B **14**, 3438 (2000).
[14] H. H. Wen, X. H. Chen, W. L. Yang, and Z. X. Zhao, Phys. Rev. Lett. **85**, 2805 (2000).
[15] Y. J. Uemura, Solid State Commun. **120**, 347 (2001).
[16] A. T. Savici, Y. Fudamoto, I. M. Gat, T. Ito, M. I. Larkin, Y. J. Uemura, G. M. Luke, K. M. Kojima, Y. S. Lee, M. A. Kastner, R. J. Birgeneau, and K. Yamada, Phys. Rev. B **66**, 014524 (2002).
[17] H. E. Mohottala, B. O. Wells, J. I. Budnick, W. A. Hines, C. Niedermayer, L. Udby, C. Bernhard, A. R. Moodenaugh, and F. C. Chou, Nat. Mater. **5**, 377 (2006).
[18] F. V. Kusmartsev, D. Di Castro, G. Bianconi, and A. Bianconi, Phys. Lett. A **275**, 118 (2000).
[19] S. A. Kivelson, G. Aeppli, and V. J. Emery, Proc. Natl. Acad. Sci. U.S.A. **98**, 11903 (2001).
[20] S. A. Kivelson, Nat. Mater. **5**, 343 (2006).
[21] J. Birgeneau, Chris Stock, John M. Tranquada, and Kazuyoshi Yamada, J. Phys. Soc. Jpn. **75**, 111003 (2006).
[22] J. M. Tranquada, *Handbook of High-Temperature Superconductivity* (Springer, New York, 2007), pp. 257–298.
[23] K. A. Müller, J. Supercond. **12**, 3 (1999); Physica C **341-348**, 11 (2000).
[24] *Superconductivity in Complex Systems*, Structure and Bonding Vol. 114, edited by K. A. Müller and A. Bussmann-Holder (Springer, Berlin, 2005).
[25] K. A. Müller, in *Intrinsic Multiscale Structure and Dynamics in Complex Electronic Oxides*, edited by A. R. Bishop, S. R. Shenoy, and S. Sridhar (World Scientific, Singapore, 2003), pp. 1–5.
[26] K. A. Müller, in *Stripes and Related Phenomena*, edited by A. Bianconi and N. L. Saini (Kluwer, New York, 2000), pp. 1–8.
[27] E. Dagotto, *Nanoscale Phase Separation and Colossal Magnetoresistance: The Physics of Manganites and Related Compounds* (Springer-Verlag, Berlin, 2003).
[28] M. Yu. Kagan and K. I. Kugel, Usp. Fiz. Nauk **171**, 577 (2001) [Phys. Usp. **44**, 553 (2001)].
[29] K. I. Kugel, A. L. Rakhmanov, and A. O. Sboychakov, Phys. Rev. Lett. **95**, 267210 (2005); A. O. Sboychakov, K. I. Kugel, and A. L. Rakhmanov, Phys. Rev. B **74**, 014401 (2006).
[30] A. O. Sboychakov, K. I. Kugel, and A. L. Rakhmanov, Phys. Rev. B **76**, 195113 (2007).
[31] A. Bianconi, G. Bianconi, S. Caprara, D. Di Castro, H. Oyanagi, and N. L. Saini, J. Phys.: Condens. Matter **12**, 10655 (2000).
[32] D. Di Castro, G. Bianconi, M. Colapietro, A. Pifferi, N. L. Saini, S. Agrestini, and A. Bianconi, Eur. Phys. J. B **18**, 617 (2000).
[33] A. Bianconi, S. Agrestini, G. Bianconi, D. Di Castro, and N. L. Saini, J. Alloys Compd. **317-318**, 537 (2001).
[34] G. Aeppli, T. E. Mason, S. M. Hayden, H. A. Mook, and J. Kulda, Science **278**, 1432 (1997).
[35] E. Dagotto, Science **309**, 257 (2005).
[36] J. Hubbard, Proc. R. Soc. London **A276**, 238 (1963); **A277**, 231 (1964).
[37] L. P. Gor'kov and G. B. Teitel'baum, Phys. Rev. Lett. **97**, 247003 (2006).
[38] V. B. Shenoy, T. Gupta, H. R. Krishnamurthy, and T. V. Ramakrishnan, Phys. Rev. Lett. **98**, 097201 (2007).
[39] U. Löw, V. J. Emery, K. Fabricius, and S. A. Kivelson, Phys. Rev. Lett. **72**, 1918 (1994).
[40] C. Ortix, J. Lorenzana, and C. Di Castro, Phys. Rev. Lett. **100**, 246402 (2008).
[41] A. O. Sboychakov, Sergey Savel'ev, A. L. Rakhmanov, K. I. Kugel, and Franco Nori, Phys. Rev. B **77**, 224504 (2008).